International Journal of Advanced Trends in Engineering and Management
(ISSN 2583-7052)

Vol. IV, No. 07, pp. 13-24, July

PSO-PI Controlled Hybrid Energy Management System for Fuel Cell Driven Electric Vehicle Applications

Thomas Thangam[1,*], A. R. Gayathri[2], E. Immanuvel Bright[3]

[1]Assistant Professor, Department of Process Engineering, International Maritime College of Oman, National University of Science and Technology, Sohar, Sultanate of Oman. thomasthangam@gmail.com
[2]Associate Professor, Department of Electrical and Electronics Engineering, Stella Mary's College of Engineering, Aruthenganvilai, Tamil Nadu, India. ar.gayu13@gmail.com
[3]Assistant Professor, Department of Electrical and Electronics Engineering, Erode Sengunthar Engineering College, Perundurai, Erode, 638057, India. immanuvelbright@gmail.com

[1*]**Corresponding Author E-mail:** thomasthangam@gmail.com

ABSTRACT: Electric Vehicles (EVs) are increasingly recognized as a more sustainable alternative to internal combustion engine vehicles due to their reduced noise levels and zero emissions. This study proposes a new energy system that combines a battery and fuel cell to power a Brushless DC (BLDC) motor for EV applications. The battery acts as an energy buffer to handle transient load demands, while the fuel cell provides high energy density and stable power output. Fuel cell voltage control and step-up conversion are accomplished via a Single-Ended Primary Inductor Converter (SEPIC). To ensure steady-state performance and fast dynamic response, a Proportional-Integral (PI) controller is implemented, with parameters optimized using Particle Swarm Optimization (PSO). A bidirectional DC-DC converter manages battery charging and discharging in response to load variations. The BLDC motor is efficiently driven under a variety of load circumstances by a three-phase Voltage Source Inverter (VSI), which converts the regulated DC output to AC. The BLDC motor is selected for its high efficiency, compact size, and minimal maintenance. The complete power management system is modeled and simulated using MATLAB/Simulink. Simulation results show that the system has a 94% energy efficiency, with an approximate rise time of 0.03 seconds, a settling time of 0.05 seconds, and an overrun of 0.03 seconds. This suggests that the system has the potential to be used in next-generation electric mobility platforms.

Keywords: Electric Vehicle, Fuel Cell, Battery, BLDC Motor, Bi-directional Converter, PI Controller, Sepic Converter.

1. Introduction

As an alternative to conventional Internal Combustion Engine (ICE) cars, EVs are becoming more and more popular due to advancements in automotive technology and rising environmental consciousness. EVs were primarily developed to reduce environmental pollution. However, modern consumers now expect enhanced reliability, greater comfort, and high performance [1].The traction motor, which is essential to power conversion, efficiency, and drivability, is at the core of EV performance. Various motor types [2], such as Permanent Magnet Motors, Induction Motors (IMs) and Switched Reluctance Motors (SRMs) have been investigated and used in electric mobility. Every variety has particular benefits and challenges [3-5]. In this work, BLDC motors are favored due to their high efficiency, fast response time, and minimal maintenance requirements. To enhance voltage and guarantee effective motor performance, a DC-DC converter is necessary, as fuel cells provide uncontrolled DC power.

DC-DC converters are essential to this process of energy control. The most popular kinds of converters for processing fuel cell output are boost and buck-boost converters. Boost converters offer simple implementation and efficient voltage step-up with minimal components. However, the Right Half Plane (RHP) zero causes non-minimum phase behavior in these systems, which makes control difficult. This limits achievable performance and complicates controller design, especially during rapid dynamic transitions [6]. Further issues that affect their scalability and dependability in automotive contexts include poor transient responsiveness, Electromagnetic Interference (EMI), excessive input current ripple, and decreased efficiency at light loads [7].

The buck-boost converter is a common option due to its ease of use and ability to regulate voltage in a range of input conditions. However, it is limited, especially when Discontinuous Conduction Mode (DCM) is used [8]. In response to these limitations, SEPIC converters have been implemented in fuel cell systems for their dual voltage regulation capability. Seamless step-up and step-down transitions are achieved while preserving output polarity, enhancing system stability.

These converters are frequently used in conjunction with PI controllers to enhance voltage regulation and dynamic response even more. For systems with nonlinearity and dynamic uncertainty, like fuel-cell-powered EVs in real-world driving scenarios, classical PI controllers are not a good fit. Improper gain tuning under varying driving profiles, load, and temperature leads to degraded controller performance. More sophisticated control optimization methods are being created to get around these restrictions [9-10]. In this work, PSO is used to optimize the PI controller's parameters. Compared to conventional tuning methods, PSO offers improved adaptability to system nonlinearities and uncertainties.

The main contributions of the proposed Fuel Cell based EV drive system are:

- Integration of SEPIC converter for efficient boosting of fuel cell voltage.
- Incorporation of PSO-PI controller for optimal converter regulation.
- Efficient energy exchange between the battery and DC bus, ensuring power supply adapts to changing load requirements.
- A PI-controlled VSI for driving the BLDC motor, providing high efficiency, quick dynamic response, and precise speed control.

2. Literature Survey

Salah Okba *et al* [2024] [11] have implemented a three-leg interleaved boost DC-DC converter for Proton Exchange Membrane Fuel Cell (PEMFC)-powered EV system. This converter topology provides enhanced flexibility in regulating the output voltage, reduces the stress on semiconductor devices by minimizing input current ripple, and optimizes the passive component specifications. However, chattering increases the fuel cell current ripple and introduces unwanted high-frequency disturbances.

Qudrat Ullah *et al* [2023] [12] have introduced a Sliding Mode Control (SMC) technique for optimal regulation of system. The model ensures a robust control by formulating a sliding surface using the tracking error between the reference and output voltage. One of the primary challenges lies in the complex mathematical formulation of the sliding surface and control law, which is difficult to design and tune.

Ahmad Saudi Samosir *et al* [2023] [13] have provided Proportional-Integral-Derivative (PID) controller for a DC-DC buck converter. The PID controller is widely used for voltage regulation in buck converters for its simplicity and ease of implementation. The PID controller struggles under rapid load transients or significant parameter variations, and its performance is highly dependent on accurate system modeling or empirical tuning.

Roberto H *et al* [2024] [14] have suggested a control technique based on Genetic Algorithms (GA) to reduce fuel consumption in the electrified propulsion system of a Mild Hybrid EV (MHEV). The GA-based approach enhances fuel efficiency by effectively managing power distribution between the internal combustion engine and the electric motor during varying driving conditions. However, it requires significant computational resources and tuning of algorithm parameters to ensure convergence.

MD. Rezanul Haque *et al* [2023] [15] have presented a DC-DC converter equipped with an enhanced PI controller that ensures precise output voltage, while minimizing overshoot resulting in reduced charging time for lithium-ion battery systems. One of the main advantages is the enhanced current regulation, which guarantees precise and steady output even with fluctuating load. Despite, modifying the conventional PI values necessitates careful consideration to prevent instability or decreased performance under various operating situations, which makes controller design and tuning more complex.

3. Proposed System Description and Modelling

This figure 1 illustrates the recommended power system architecture, which powers a BLDC motor with a battery and fuel cell. The block diagram presents the proposed power system configuration for a BLDC motor that uses coordinated energy input from a battery and a fuel cell.

The BLDC motor, which is the central component of the system, is driven by a regulated DC power supply. The primary source of this electricity is the fuel cell, which produces DC voltage and current suitable for propulsion applications. A DC-DC SEPIC converter is employed to process the fuel cell's output and boost the voltage to the level required by the motor. A PSO-PI controller is employed to improve the accuracy of voltage regulation and enhance the transient response. The SEPIC converter maintains the desired output voltage even under varying load conditions, as its controller is optimally tuned using PSO. Furthermore, a bidirectional DC-DC converter enables the battery to serve as an additional energy source during times of high demand.

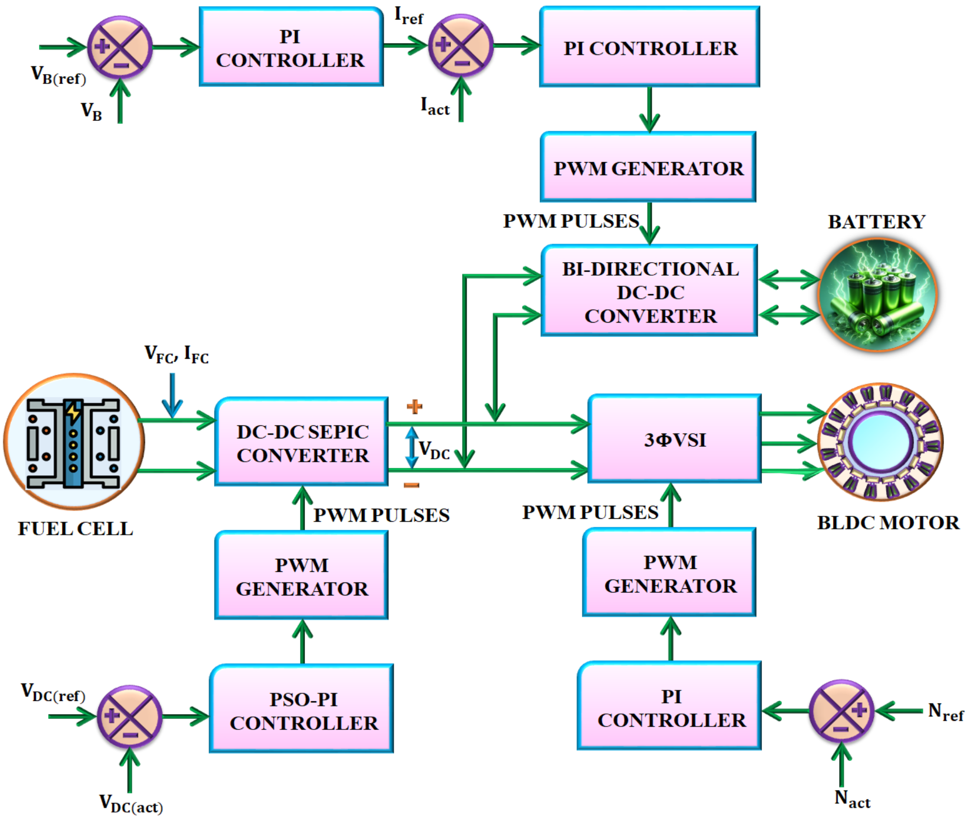

Figure 1: *Block diagram of proposed system*

In addition, a specialized PI controller and PWM generator manage the bidirectional DC-DC converter, ensuring efficient charging and discharging cycles in response to system requirements. Control loops are used to continuously monitor and compare feedback signals, such as voltage, current, and motor speed, with reference values. This closed-loop technique ensures accurate motor control, dependable energy balance, and overall power system efficiency.

3.1 Fuel Cell Structure

Electrochemical fuel cells operate on the basis of electrochemical energy conversion principle, which directly transforms the chemical energy of hydrogen (fuel) and oxygen (oxidant) into electrical energy. Fuel cells depend on an external fuel supply to produce electricity, in contrast to electrochemical storage devices that store and release energy internally, shown in Figure 2.

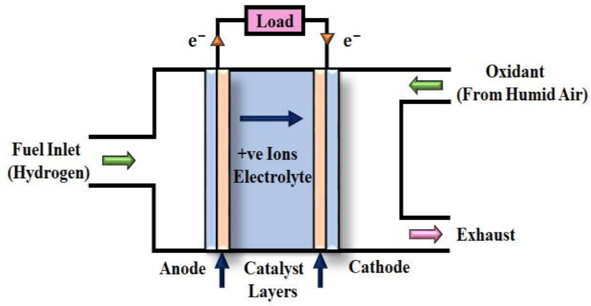

Figure 2: *Fuel cell structure*

In particular, the great energy efficiency, small size, affordability, and ideal operating temperature of PEM fuel cells make them ideal for automobile applications. Other varieties include alkaline fuel cells, which are usually used in spacecraft, and solid oxide fuel cells, which are utilized for fixed backup power. Fuel cells produce only water as a by-product, making them a clean and combustion-free alternative to ICEs. At the moment, reforming is the main method used to create hydrogen as shown in Equation (1)

$$Methane + Steam \rightarrow Hydrogen + Carbon\ monoxide \quad (1)$$

3.1.1 Operating Principle

The three primary parts of a fuel cell are an electrolyte, a cathode, and an anode. Equation (2) illustrates how hydrogen gas oxidizes at the anode and splits into H^+ ions and electrons when a catalyst is present.

$$H_2 \rightarrow 2H^+ + 2e^- \quad (2)$$

The produced H^+ ions travel to the cathode through the polymer electrolyte membrane. At the same time, electrons produce DC electrical energy as they flow through an external circuit. Reduction occurs at the cathode, where oxygen, H+ ions, and electrons mix to create water and emit heat, as shown by Equation (3):

$$1/_2\, O_2 + 2H^+ + 2e^- \rightarrow H_2O \quad (3)$$

To improve overall efficiency and maintain a stable power supply, fuel cells are paired with SEPIC converters.

3.2 DC-DC Sepic Converter

The SEPIC DC-DC converter's CCM operation is shown in figure 3.In input voltage source (V_{FC}), two inductors (L_1 and L_2), a power diode (D), an output filter capacitor (C_2), and a switching device (often an Insulated Gate Bipolar Transistors (IGBT)) labeled S_1 comprise the circuit. The circuit additionally has a load resistor *(R)*. In addition to ensuring that current flows continuously in the DC channel, the coupling capacitor (C_1) also acts as an electrical isolation device between the input and output stages.

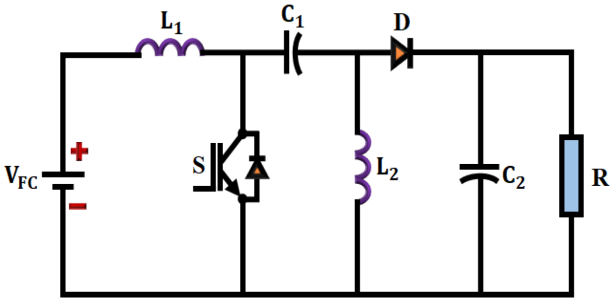

Figure 3: *Circuit diagram for a SEPIC DC-DC converter*

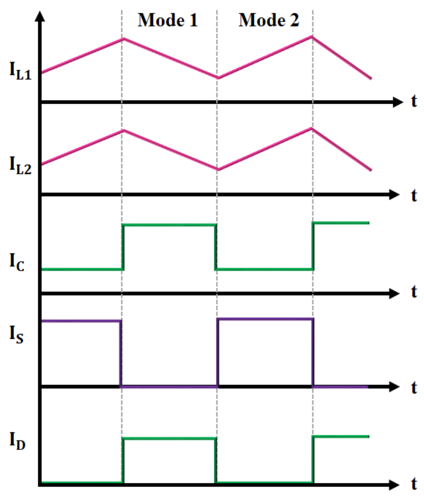

Figure 4: *Switching waveform of SEPIC converter*

The operation of CCM, which is the subject of this study, is distinguished by two main switching states, which are explained below.

3.2.1 SEPIC converter operating modes

Mode 1: When activating switch S, the current flowing through the first inductor, I_{L1}, rises. At the same time, the second inductor I_{L2}, experiences a rise in current as well, but it flows in the other direction. This contributes to greater energy storage in L_1, the first inductor. Capacitor C_1 provides energy to aid in raising the current in I_{L1} throughout this procedure. As seen in figure 5, this explains the SEPIC converter's operating state when switch S is ON.

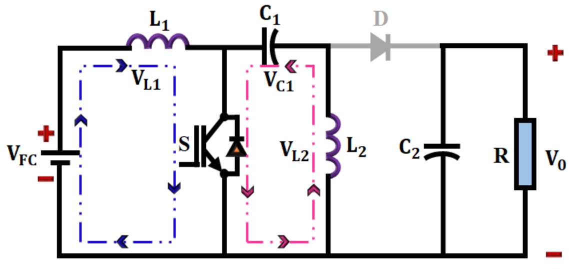

Figure 5: *SEPIC converter operation mode 1*

The equations (4), (5), (6), and (7) that relate to mode 1 of CCM employing Kirchhoff's Voltage Law (KVL) and Kirchhoff's Current Law (KCL) are displayed.

$$V_{FC} - L_1 \frac{di_{L1}}{dt} = 0 \quad (4)$$

$$C_1 \frac{dV_{C1}}{dt} + i_{L1} = 0 \quad (5)$$

$$L_2 \frac{di_{L2}}{dt} - V_{C1} = 0 \quad (6)$$

$$C_2 \frac{dV_{C2}}{dt} + \frac{V_{C2}}{R} = 0 \quad (7)$$

Mode 2: When switch S is off, the currents through inductor (I_{L1}) and capacitor (I_{C1}) are equal. Meanwhile, the current through the second inductor (I_{L2}) continues flowing in same direction. At this moment, diode D is conducting. Figure 6 shows the SEPIC converter operating in this mode with switch S turned off.

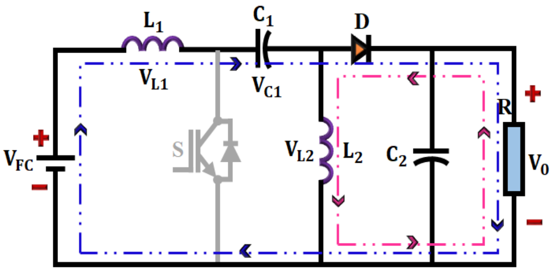

Figure 6: *SEPIC converter operation mode 2*

Equations (8), (9), (10), and (11) display the relevant equations to mode 2 of CCM using KVL and KCL.

$$V_{FC} = L_1 \frac{di_{L1}}{dt} + V_{C1} + V_{C2} \quad (8)$$

$$L_2 \frac{di_{L2}}{dt} + V_{C2} = 0 \quad (9)$$

$$C_1 \frac{dV_{C1}}{dt} - i_{L1} = 0 \quad (10)$$

$$C_2 \frac{dV_{C2}}{dt} - i_{L1} - i_{L2} + \frac{V_{C2}}{R} = 0 \quad (11)$$

The volt-second balance principle states that the average voltage across the inductor over a complete switching cycle is zero for converters operating under steady-state conditions. Practical elements such as diode and switch voltage drops are included in the circuit analysis to improve accuracy. The inductor voltage is$(V_{L1} = V_{FC} - V_{C1} - V_D - V_O)$, and the voltage across inductor L_1 is $(V_{L1} = V_{FC})$ during the first window of the switching time,$(D_T < t \leq T)$. Equation (12) is derived by applying volt-second balance over the switching cycle and setting the average inductor voltage to zero.

$$\frac{1}{T}\left(\int_0^T V_{L1} dt\right) = \frac{1}{T}\left[\int_0^{DT} V_{FC}\, dt + \int_{DT}^{T} (V_{FC} - V_{C1} - V_D - V_O) dt\right] = 0 \quad (12)$$

Equation (13) is obtained by rearranging the following equations and finding the integral.

$$V_{C1} + V_D + V_O = \frac{V_{FC}}{1-D} \quad (13)$$

Similarly, when inductor L_2 is subjected to the volt-second balancing, the voltage across L_2 within the interval $(0 < t \leq D_T)$ is $(V_{L2} = V_{C1})$. When$(D_T < t \leq T)$, the voltage across L_2 is $V_{L2} = -V_O + V_D$, which results in equation (14).

$$\frac{1}{T}\left(\int_0^T V_{L1} dt\right) = \frac{1}{T}\left[\int_0^{DT} V_{C1}\, dt + \int_{DT}^{T} (-V_O - V_D) dt\right] = 0 \quad (14)$$

$$V_{C1} + V_O + V_D = \frac{V_O + V_D}{D} \quad (15)$$

Combining (13) and (15) yields the SEPIC converter's transfer ratio or voltage gain (G) in terms of (D), as indicated in (16).

$$G = \frac{V_O + V_D}{V_{FC}} = \frac{D}{1-D} \quad (16)$$

The duty cycle value (D) determines whether the value of (G) is more than or less than one. Better voltage regulation is achieved using PSO-optimized PI controller, which enhances response time, accuracy, and stability.

3.3 PSO Based PI Controller

The PI controller adjusts the control signal using both present and past error values to maintain accuracy and stability. Manual tuning of PI gains (K_p) and (K_i) often leads to suboptimal performance in nonlinear or time-varying systems. PSO uses a population-based search to determine optimal controller parameters by minimizing an error-based objective function. It efficiently explores the solution space without relying on gradient information. The integrated PSO-PI controller ensures adaptive tuning, delivering faster response, minimal error, and enhanced system robustness.

$$G_{PI}(s) = K_p + \frac{K_i}{s} \tag{17}$$

Equation (17) represents the PI controller in the Laplace domain, where $K_p$the present error response, and K_i accounts for the accumulated past error to eliminate steady-state error.

$$e(t) = V_{ref} - V_o(t) \tag{18}$$

Equation (18) defines the real-time control error as the difference between the reference output V_{ref} and the actual system output $V_o(t)$.

$$u(t) = K_p.e(t) + K_i.\int_0^t e(T)dT \tag{19}$$

Equation (19) describes the time-domain output of the PI controller, where *u(t)* is the control signal, *e(t)* is the error, K_p is the proportional gain, and K_i is the integral gain.

$$V_i^{(t+1)} = \omega V_i^{(t)} + c_1 r_1\left(P_{best,i} - X_i^{(t)}\right) + c_2 r_2\left(G_{best} - X_i^{(t)}\right) \tag{20}$$

The velocity update equation in PSO is composed of three primary components: inertia, cognitive, and social behavior. The inertia term, $\omega V_i^{(t)}$, retains part of the particle's previous velocity to maintain momentum and avoid abrupt changes. The cognitive component, $c_1 r_1\left(P_{best,i} - X_i^{(t)}\right)$, directs the particle toward its own best historical position, allowing it to exploit personal learning. In parallel, the social component, $c_2 r_2\left(G_{best} - X_i^{(t)}\right)$, guides the particle based on the collective knowledge of the swarm.

Figure 7 shows the flowchart for the proposed PSO-based PI controller. It begins with initializing PSO parameters and assigning swarms as candidate K_p and $K_i$values for the PI controller. The fuel cell-powered EV system is then simulated to compute the initial objective function, typically based on performance indices like Mean Error Square (MES). In each iteration, particles update their velocity and position using personal best (P_{best}) and global best (G_{best}) values, refining the controller gains. The loop continues until convergence, yielding optimal PI parameters that ensure smooth power management and dynamic stability for the fuel cell EV system.

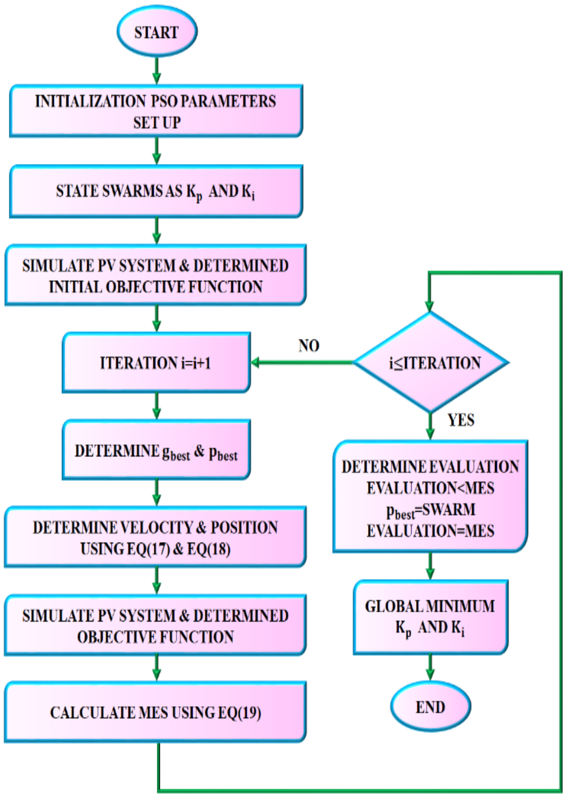

Figure 7: *Flow chart of PSO optimization algorithm for optimal PI controller*

The PSO-PI controller is applied to BLDC motor control in fuel cell electric vehicles to achieve optimal speed and torque regulation. PSO dynamically tunes the PI gains to adapt to nonlinearities and load variations in real-time. This ensures efficient motor performance, smooth acceleration, and enhanced energy utilization from the fuel cell source.

3.4 BLDC Motor

The BLDC motor is capable of being analyzed using a variety of models. In this study, the phase variables (abc) approach a simple and efficient method for creating BLDC motor control systems is the foundation for the BLDC motor modeling. The stator winding resistance, inductance, and Back Electromotive Force (Back-EMF) are typically connected in series to mimic a three-phase BLDC motor, as shown in figure 8.

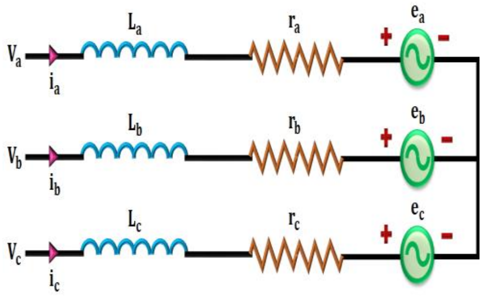

Figure 8: *Equivalent circuit of the BLDC motor*

The model is predicated on the following assumptions for simplicity: the air gap is uniform; the magnetic circuit is unsaturated; hysteresis and eddy current losses are disregarded; and the three stator phases are identical and symmetrical. Consequently, the BLDC motor's voltage equations are shown in equation (21).

$$\begin{bmatrix} V_a \\ V_b \\ V_c \end{bmatrix} = \begin{bmatrix} r_a & 0 & 0 \\ 0 & r_b & 0 \\ 0 & 0 & r_c \end{bmatrix} \begin{bmatrix} i_a \\ i_b \\ i_c \end{bmatrix} + \frac{d}{dt} \begin{bmatrix} L_a & M_{ab} & M_{ac} \\ M_{ba} & L_b & M_{bc} \\ M_{ca} & M_{cb} & L_c \end{bmatrix} \begin{bmatrix} i_a \\ i_b \\ i_c \end{bmatrix} + \begin{bmatrix} e_a \\ e_b \\ e_c \end{bmatrix} \quad (21)$$

The phase voltages are V_a, V_b, and V_c; the stator winding resistances are r_a, r_b, and r_c; the mutual inductances of the stator windings are L_a, L_b, and L_c; the phase currents are i_a, i_b, and i_c; and the back-EMF voltages are e_a, e_b, and e_c.

Based on the aforementioned assumptions, it is inferred that $L_a = L_b = L_c = L, r_a = r_b = r_c = r$ and $M_{ab} = M_{bc} = M_{ca} = M$.

The three-phase winding is also connected in a star, which allows for the following simplification to be mentioned:

$$i_a + i_b + i_c = 0 \Longrightarrow i_b + i_c = -i_a \quad (22)$$

$$L_{ia} + M_{ib} + M_{ic} = L_{ia} + M(-i_a) = (L - M)i_a \quad (23)$$

Therefore, equation (21) becomes once the same mathematical processes are repeated for the other two phases.

$$\begin{bmatrix} V_a \\ V_b \\ V_c \end{bmatrix} = \begin{bmatrix} r & 0 & 0 \\ 0 & r & 0 \\ 0 & 0 & r \end{bmatrix} \begin{bmatrix} i_a \\ i_b \\ i_c \end{bmatrix} + \frac{d}{dt} \begin{bmatrix} L_s & 0 & 0 \\ 0 & L_s & 0 \\ 0 & 0 & L_s \end{bmatrix} \begin{bmatrix} i_a \\ i_b \\ i_c \end{bmatrix} + \begin{bmatrix} e_a \\ e_b \\ e_c \end{bmatrix} \quad (24)$$

Where the analogous phase inductance is represented by $L_s = L - M$.

To analyze the motor's speed, it is essential to first establish its mechanical equations. The following is an expression for the speed derivative and electromagnetic torque:

$$T_e = T_L + J\frac{d\Omega}{dt} + B\Omega \quad (25)$$

$$T_e = \frac{i_a e_a + i_b e_b + i_c e_c}{\Omega} \quad (26)$$

The resistive torque is denoted by T_L, the moment of inertia by J, the coefficient of friction by B, and the mechanical speed of the motor (rad/s) by d.

A BLDC motor drive converted to a bidirectional converter allows energy flow in both directions supplying the motor during acceleration and returning energy to the source during deceleration. This process recovers energy otherwise lost, thereby increasing overall system efficiency. It also enhances system reliability by improving power control and reducing stress on components.

3.5 Bi-Directional Converter

The bidirectional, non-isolated DC-DC converters chosen for this study are displayed in figure 9. In this system, bidirectional power flow is made possible by replacing the diodes with controlled switches.

- In buck mode, which operates forward, switch S_1 is activated.
- In boost mode, which operates backwards, switch S_2 is activated.

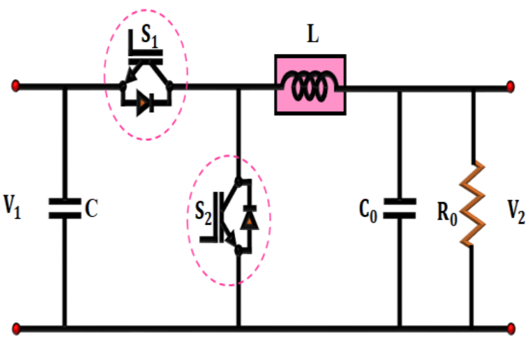

Figure 9: *Circuit for bidirectional DC-DC converter*

3.5.1 Buck mode (Forward operation):

During buck mode, the output voltage remains below the input voltage. To initiate battery charging from the DC grid, switch S_1 is activated while switch S_2 remains off, as illustrated in figure 10.When $S_1$is activated, the input current increases and flows via the inductor L as well as S_1. When S_1 is turned off, the current flowing through the inductor decreases until the next switching cycle begins. During this time, the energy stored in the inductor L is used to charge the battery.

The duty cycle of the switch, taking into account the estimated efficiency, is expressed by the following equation (27).

$$D = \frac{V_{OUT}}{V_{IN \times \eta}} \quad (27)$$

3.5.2 Boost mode (Backward Operation):

The output voltage is greater than the input voltage when in boost mode. In this mode, switch S_1 stays off while switch S_2 is turned on, allowing the battery to power the load.

When switch S_2 is turned on, the input current increases and flows through the inductor and switch S_2. The inductor's current decreases until the next cycle starts when S_2 is turned off. The load then receives the energy that was previously stored in the inductor L.

$$D = 1 - \frac{V_{IN \times \eta}}{V_{OUT}} \quad (28)$$

The switch's duty cycle, adjusted for the estimated efficiency, is shown in equation (28).

The detailed system modelling ultimately provides profound understanding of the dynamics of the converter and motor, which forms an essential foundation for accurate control and improved drive performance optimization.

4. Results and Discussion

In the section the outcomes attained using MATLAB simulation is discussed together with Table 1 detailing the specification of system components.

Table 1: *Specification Table*

Parameter	Rating
SEPIC CONVERTER	
Switching frequency	$10kHz$
Inductor L_A, L_B	$4.7mH$
Capacitor C_C	$22\mu F$
Capacitor C_O	$2200\mu F$

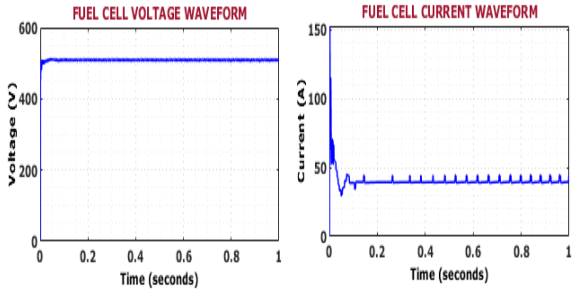

Figure 10: *Fuel cell voltage and current waveforms*

The fuel cell voltage and current waveforms derived from the simulation are shown in figure 10. The voltage waveform exhibits a steady-state operation, with a sharp rise followed by stabilization at around 450 V. The current waveform shows a brief spike before settling at approximately 38 A, with slight oscillations indicating dynamic load behavior. The results confirm that the fuel cell system performs reliably and consistently under various operating conditions.

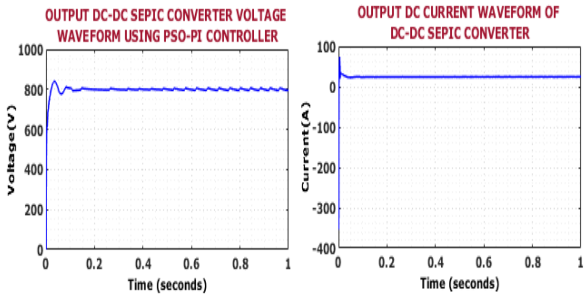

Figure 11: *Output voltage and current waveforms of DC-DC SEPIC converter*

As shown in figure 11, the DC-DC SEPIC converter governed by the PSO-PI controller produces output voltage and current waveforms characterized by fast transient response and stable behavior, with the voltage swiftly settling near 800 V and exhibiting low ripple. The current waveform shows strong regulation under steady-state conditions, first spiking and then stabilizing at about 20 A. The PSO-PI controller's ability to achieve rapid convergence and steady operation is validated by these results.

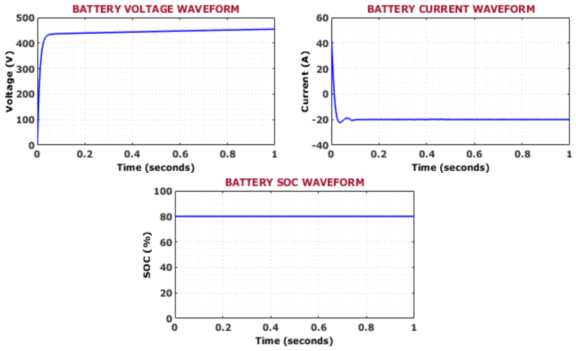

Figure 12: *Battery waveforms*

Battery voltage, current, and state of charge waveforms during operation are shown in figure 12. Efficient charging is indicated by the voltage waveform, which climbs rapidly and stabilizes at about 450 V. Charging mode is confirmed by the current waveform, which displays an initial transient followed by a continuous negative value close to -20 A. Stable energy storage with minimal variations is reflected by the SOC waveform, which stays steady at 90%.

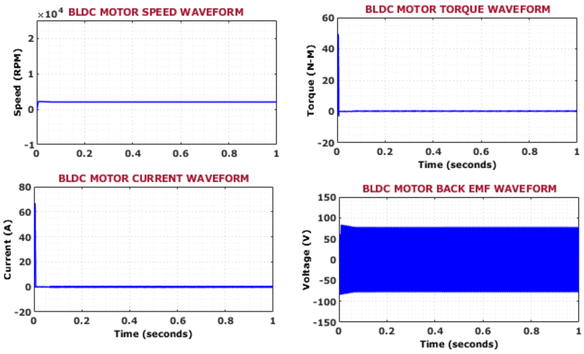

Figure 13: *BLDC motor waveforms*

Figure 13 displays the performance waveforms of BLDC motors, showing parameters like speed, torque, current, and back EMF. The motor reaches a steady speed of about 2000 RPM within 1 second, as indicated by the speed waveform. The torque waveform remains constant close to zero, suggesting minimal load conditions. The current waveform starts with a high peak due to the initial inrush current and quickly settles around 10 A, indicating steady-state operation. The back EMF waveform shows a steady sinusoidal voltage pattern, which is characteristic of proper BLDC motor functionality.

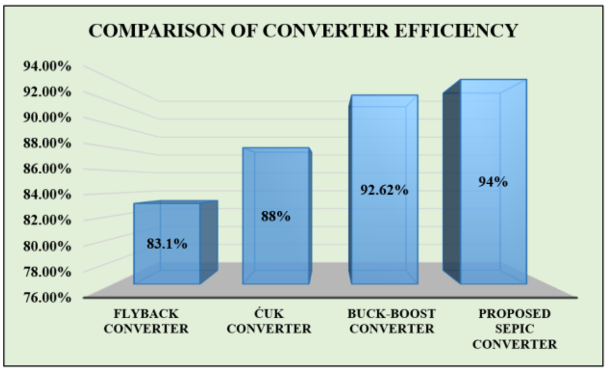

Figure 14: *Comparison of converter*

Figure 14 compares the efficiency of four distinct DC-DC converter types. At 83.1%, the Flyback converter has the lowest efficiency, mostly due to increased switching losses and magnetic complexity [16]. The Cuk converter benefits from continuous input and output currents, operating with a moderate efficiency of 88% [17]. The Buck-Boost converter's streamlined topology and efficient control enable it to achieve a higher efficiency of 92.62% [18]. The proposed SEPIC converter, with the highest efficiency of 94%, avoids output ripple and voltage instability, making it ideal for fuel cell–battery integration.

Table 2: *Comparative analysis of control algorithms*

Models	Rise Time (t_r)	Settling Time (t_s)	Overshoot
FUZZY-PID [19]	0.01	0.20	1.0
FOPI [20]	0.557	3.2	0.525
Proposed	0.03	0.05	0.03

Table 2 provides a comparative analysis of time-domain response characteristics for three different controllers: FOPI, FUZZY-PID, and the proposed PSO-PI. The FUZZY-PID controller exhibits the shortest rise time of 0.01 s but is limited by its higher overshoot and prolonged settling period [19]. The FOPI controller exhibits moderate performance, with a rise time of 0.557 s, a settling time of 3.2 s, and an overshoot of 0.525 [20]. In comparison, the proposed PSO-PI controller offers significantly improved results, achieving a balanced rise time of 0.03 s, a rapid settling time of 0.05 s, and the smallest overshoot of just 0.03.

5. Conclusion

In this paper, a PSO-tuned PI controller for electric motor applications is designed and successfully implemented in a fuel cell–battery integrated power system. A DC-DC SEPIC converter is integrated into the system to effectively boost and stabilize the fuel cell voltage, ensuring continuous and reliable power output. By employing a PSO-based tuning technique, the PI controller enhances dynamic response and voltage regulation under various load scenarios. A bidirectional converter effectively oversees battery charging and discharging processes, maintaining energy balance within the system. These coordinated control strategies ensure smooth and stable operation of the BLDC motor. The system's performance is confirmed by the MATLAB/Simulink simulation, which shows a 0.03 overshoot, a rising time of around 0.03 seconds, a settling time of roughly 0.05 seconds, and 94% energy efficiency. The results validate that the proposed control method is both robust and suitable for advanced electric motor applications, especially in the context of EVs.

Reference

1. Jiman Kim; Hyunsu Kim, Year: 2024, “Design of electronic filter for noise and vibration reduction in brushed DC Motor”, Machines, Vol: 12, No: 3, pp. 148.

2. K.S. Kavin; P. Subha Karuvelam, Year: 2023, “PV-based grid interactive PMBLDC electric vehicle with high gain interleaved DC-DC SEPIC Converter”, IETE Journal of Research, Vol: 69, No: 7, pp. 4791 – 4805.

3. H. Vidhya; I. Abinaya; M. Karthik; RR Rubia Gandhi, Year: 2019, “FLC based Speed Control of Brushless DC Motor using C2000,” International Journal of Research in Engineering, Science, and Management, Vol: 2.

4. Ali Abdel-Aziz; Mohamed Elgenedy; Barry Williams, Year: 2024, “The switched reluctance motor converters and torque ripple minimisation techniques for electric vehicle applications”, Energies, Vol: 17, No: 13, pp. 3263.

5. Abinaya I; R. R Rubia Gandhi; H. Vidhya; M. Karthik; R. Thangaraj, “Demand Side Management for Motoring and Lighting Loads”, International Journal of Research in Engineering, Science and Management.

6. R. Rubia Gandhi, I. Abinaya, H. Vidhya, M. Karthik, Year: 2019, “Sensor less speed control of Brushless DC motor using fuzzy logic controller International journal of novel research and development”, Vol: 4, No: 5.

7. Hasan Mollaee; Seyyed Morteza Ghamari; Fatemeh Khavari, Year: 2022, “Self-tuning regulator adaptive controller design for DC-DC boost converter with a novel robust improved identification method”, IET Power Electronics, Vol: 15, No: 13, pp. 1365 – 1379.

8. K. S. Kavin; P. Subha Karuvelam; R. Tharwin Kumar; M. Sivasubramanian; P. Kavitha; S. Priyadharsini, Year: 2023, “GWO Optimized PI Controller Fed PV Based Interleaved Luo Converter for EV Applications”, In 2023 14th International Conference on Computing Communication and Networking Technologies (ICCCNT), pp. 1 – 6. IEEE.

9. Timothy Frei; Ching-Hsiang Chang; Maurice Filo; Asterios Arampatzis; Mustafa Khammash, Year: 2022, “A genetic mammalian proportional–integral feedback control circuit for robust and precise gene regulation”, Proceedings of the National Academy of Sciences, Vol: 119, No: 00 ,pp. e2122132119.

10. Gowthamraj Rajendran; Chockalingam Aravind Vaithilingam; Kanendra Naidu; Ahmad Adel Alsakati; Kameswara Satya Prakash Oruganti; Mohd Faizal Fauzan, Year:2022, “Dynamic voltage stability enhancement in electric vehicle battery charger using particle swarm optimization”, IEEE Access, Vol: 10, pp. 97767 – 97779.

11. Salah Okba; Ramzi Saadi; Mohamed Yacine Hammoudi; Yassine Himeur; Abir Betka; Shadi Atalla; Wathiq Mansoor, Year: 2024, “Duel loop FOPI controller based Equilibrium Optimizer tuning approach for three-phase interleaved boost converter; PEMFC HEVs”, IEEE Access, vol: 12, pp. 129511 – 129527.

12. Qudrat Ullah; Tiago Davi Curi Busarello; Danilo Iglesias Brandao; Marcelo Godoy Simões, Year: 2023, “Design and performance evaluation of SMC-based dc–dc converters for microgrid applications”, Energies, vol: 16, No: 10, pp. 4212.

13. Ahmad Saudi Samosir; Tole Sutikno; Luthfiyyatun Mardiyah, Year: 2023, “Simple formula for designing the PID controller of a DC-DC buck converter”, International Journal of Power Electronics and Drive Systems, Vol: 14, No: 1, pp. 327.

14. Roberto HQ Filho; Rodrigo PM Ruiz; Eisenhawer de M. Fernandes; Rosalvo B. Filho; Felipe C. Pimenta, Year: 2024, “Development of a Genetic Algorithm-Based Control Strategy for Fuel Consumption Optimization in a Mild Hybrid Electrified Vehicle’s Electrified Propulsion System”, Energies, vol: 17, No: 9, pp. 2015.

15. Md Rezanul Haque; K. M. A. Salam; Md Abdur Razzak, Year: 2023, “A Modified PI-Controller Based High Current Density DC–DC Converter for EV Charging Applications”, IN IEEE Access, Vol: 11, pp. 27246 – 27266.

16. Yuchao Huang; Kui Yan; Qidong Li; Xiangyi Song; Desheng Zhang; Qiao Zhang, Year: 2024, “Very-High-Frequency Resonant Flyback Converter with Integrated Magnetics”, Electronics , Vol: 13, No: 22, pp. 4363.

17. Khaled A. Mahafzah; Ali Q. Al-Shetwi; M. A. Hannan; Thanikanti Sudhakar Babu; Nnamdi Nwulu, Year: 2023, “A new Cuk-based DC-DC converter with improved efficiency and lower rated voltage of coupling capacitor”, Sustainability, Vol: 15, No: 11, pp. 8515.

18. Majid Hosseinpour; Mahsa Ahmadi; Ali Seifi; Seyed Hossein Hosseini, Year: 2024, “A new transformerless buck-boost converter with improved voltage gain and continuous input current”, IET Power Electronics, Vol: 17, No: 4, pp. 534 – 550.

19. Yuru Jia; Zhang RUliang; Lv Xue; Tao Zhang; Zhengwu Fan, Year: 2022, “Research on Temperature Control of Fuel-Cell Cooling System Based on Variable Domain Fuzzy PID [J]”, Processes, Vol: 10, No: 3, pp. 534.

20. Deepti Thaliyadath; Deepa Kaliyaperumal; Mohan Lal Kolhe, Year: 2024, “Enhancing transient response in a DC-DC converter for electric vehicle DC fast charging applications using fractional-order PI control”, Energies, Vol: 17, No: 17, pp. 4312.